Vol. 14, pp. 1–11 (2017)
doi: 10.2142/biophysico.14.0_1

Biophysics and Physicobiology
https://www.jstage.jst.go.jp/browse/biophysico/

Regular Article

Mechanical properties of spindle poles are symmetrically balanced

Kazuya Suzuki[1,2], Takeshi Itabashi[1,2] and Shin'ichi Ishiwata[1]

[1]*Department of Physics, Faculty of Science and Engineering, Waseda University, Shinjuku-ku, Tokyo 169-8555, Japan*
[2]*Waseda Bioscience Research Institute in Singapore (WABIOS), 11 Biopolis Way, Singapore 138667, Singapore*

Received October 14, 2016; accepted November 28, 2016

The metaphase spindle is organized for accurate chromosome segregation. One of the fundamental features of the spindle across the species is its symmetrical shape; the spindle consists of two polar arrays of microtubules at both ends. Although it has been suggested that the formation of the bipolar shape requires force balance coordination by molecular motors, i.e., kinesins and dyneins, quantitative analysis for the pole mechanics has not been conducted. Here, we demonstrate that it is not only the shape but also the stiffness and microtubule density of the pairs of pole regions are symmetrically balanced in single spindles self-assembled in *Xenopus* egg extracts. We found that the inhibition of dynein functions dramatically reduced the stiffness and microtubule density in the pole region. By contrast, the inhibition of one of the kinesins, Eg5, which is the antagonistic motor protein of dynein, increased the value of these parameters. Moreover, the inhibition of both dynein and Eg5 recovered these parameter values to those of non-treated spindle poles. We also found that, when one pole structure was held widened with the use of two glass microneedles, the opposite pole structure spontaneously widened, resulting in the formation of the barrel-like shaped spindle. The values of stiffness and microtubule density in the manipulated pole region decreased, following the spontaneous decrement of those in the paired unmanipulated pole region. These results suggest that the spindle possesses a mechanism to dynamically maintain its symmetry in mechanical properties.

Key words: spindle, microtubule, molecular motors, micromechanics, symmetry

Corresponding author: Shin'ichi Ishiwata, Department of Physics, Faculty of Science and Engineering, Waseda University, 3-4-1 Okubo, Shinjuku-ku, Tokyo 169-8555, Japan.
e-mail: ishiwata@waseda.jp

The spindle pole consists of microtubules, molecular motors including kinesins and dyneins, and various microtubule-associated proteins (MAPs) [1,2]. The spindle poles maintain their shape during metaphase, although pushing and pulling forces are applied at every moment by microtubule polymerization and depolymerization, and by molecular motors [3]. Morphological abnormality of the pole causes chromosome aberration [4–6], thus the pole structure must be sufficiently rigid to endure those forces.

Recently, quantitative analyses of the micromechanics for the overall spindle structure have been conducted by examining the responses of the spindle to mechanical perturbations using cantilevers or glass microneedles [7–10]. Shimamoto *et al.* [8] showed that the elasticity of the overall spindle structure was dramatically reduced when the pole

◀ **Significance** ▶

Although spindle pole structure has been suggested to determine the mechanical properties of the overall spindle structure, quantitative analysis for the pole mechanics has not been performed. Here, we demonstrate that the mechanical properties including shape, stiffness and microtubule density of pairs of pole regions are symmetrically balanced in single spindles. We found that, when the one pole region was widened with two microneedles, the other pole region was spontaneously widened to form a barrel-like shape. These results suggest that the spindle symmetry in mechanical properties is dynamically maintained.

structures were disrupted by inhibition of the dynein functions, however, interestingly when the pole structures were restored by additional inhibition of Eg5 (a tetramer of kinesin-5) activities, the elasticity of the overall spindle structure was recovered compared to that in the absence of the inhibitors. Thus, the mechanical properties can be established by multiple, possibly redundant, mechanisms.

Those mechanical perturbation experiments clarified the spindle micromechanics quantitatively, and moreover, they demonstrated the unique spindle responses to external forces. That is, when the spindle width was reduced by cantilever-induced compression, the spindle length spontaneously decreased, so that its aspect ratio recovered to that of unperturbed spindles [7,9]. When the spindle length was extended by applying the stretching force with a pair of glass microneedles, the spindle width decreased. After the stretching, the width spontaneously increased and the original spindle shape was nearly recovered [9,10]. Taken together, although the mechanism has not yet been clarified, the spindle intrinsically possesses the characteristics of maintaining its shape and size so as to adapt to external forces.

Contrary to the micromechanics and mechanical responses of the overall spindle structure, those of the pole structure remain elusive. In this study, using glass microneedles, we examined the micromechanics and mechanical response of the pole regions in metaphase spindles that were self-assembled in *Xenopus* egg extracts. Unlike the spindles organized in somatic cells, these spindles can self-assemble in the egg extract without centrosomes, providing a unique context for studying the roles of molecular motors in the pole mechanics.

Materials and Methods

Spindle assembly in *Xenopus* egg extracts

Xenopus egg extracts were prepared as reported previously [11]. The extracts were arrested at metaphase, and then entered into interphase by the addition of $CaCl_2$ at 0.3 mM. Demembranated *Xenopus* sperm nuclei were incubated in the interphase extracts for 80 min, and they formed interphase nuclei. After the addition of fresh metaphase extracts, these extracts were incubated for 1 h to organize metaphase spindles. All experiments were conducted at 20 ± 2°C. All procedures conformed to the "Guidelines for Proper Conduct of Animal Experiments" approved by the Science Council of Japan, and were performed according to the regulations for animal experimentation at Waseda University.

Micromanipulation of spindles

Glass microneedles were fabricated by pulling glass rods (G1000, Narishige, Tokyo, Japan) using a capillary puller (PC-10, Narishige) and a microforge (MF-900, Narishige). The diameter of the needle tip was 1–2 μm. A flexible needle (0.3–1.0 nN/μm) was created and calibrated as described previously [10,12]. These needles were not passivated as reported previously [10]. The movement of the needles was controlled by two micromanipulators (MHW-3, Narishige), one of which was equipped with a piezo actuator (P-841.20, PI Japan, Tokyo, Japan). In all of the experiments, the stiff needle was moved at 1 μm/sec. The stiffness of a pair of pole regions was measured as follows: after the measurement of one pole region, that of the other was measured within 1 min. Similarly, the stiffness of the pole region was measured within 1 min after the measurement of the stiffness of the midzone region. Note that, when the midzone stiffness was measured, the pole stiffness measurement was taken in only one pole region, not in two pole regions. This is because it is difficult to quickly conduct three successive stiffness measurements (two pole regions and one midzone region) in a single spindle.

Egg extracts containing metaphase spindles were spread onto a siliconized coverslip (custom ordered, Matsunami Glass, Osaka, Japan) coated with Pluronic F-127 (P2443, Sigma-Aldrich, St. Louis, Missouri, USA) as reported previously [10,13]. The extracts were covered with mineral oil (M-5310, Sigma-Aldrich) to prevent evaporation [10,13,14].

Microscopy and image analysis

Fluorescence and bright field images were acquired using a charge-coupled device (CCD) camera (AxioCam MRm, Carl Zeiss, Oberkochen, Germany) and an upright microscope (Axio Imager, Carl Zeiss) equipped with a 40× objective (0.75 NA, Carl Zeiss), or a Hamamatsu ORCA-AG CCD camera (Hamamatsu Photonics, Shizuoka, Japan) or an electron multiplying EM-CCD camera (iXon EM+, Andor Technology, Belfast, UK) mounted on an inverted microscope (IX71, Olympus, Tokyo, Japan) with a 60× UPlanSApo lens (1.35NA, Olympus) and a confocal scanning unit (CSU10, Yokogawa, Tokyo, Japan). AxioCam MRm camera was used to acquire the images of the spindles shown in Supplementary Figure S2A. Hamamatsu ORCA AG and iXon EM+ cameras were used for acquiring the images of the spindles and the needles during the measurement of the stiffness. Note that, for the measurement of microtubule density, only iXon EM+ camera was used for acquiring the images. Image acquisition was performed with Andor iQ software (Andor Technology). For time-lapse observation, images were acquired over 10 sec, and three-dimensional (3D) scanning was usually performed every 5 min. To visualize spindles, we added ~20 μg/ml of either tetramethylrhodamine (C-1171, Life Technologies, Carlsbad, CA, USA) or Alexa-488 (A-20000, Life Technologies) -labeled tubulin [15], or both, depending on the experiment, to the extracts. Microtubule density was estimated from the fluorescence intensity measured by 3D observation of a spindle, as reported in our previous work [10,13]. We adopted the same definition for the boundary of the spindle as that in our previous works; in the fluorescence images, we defined a voxel where the fluorescence intensity was at least 1.5 fold that of cytoplasm to be a voxel where the spindle microtubules exist.

The spindle size and the displacement of the needles were determined by ImageJ (National Institute of Health, Bethesda, MD). The statistical significance of the data was evaluated by Mann–Whitney *U* test for Figure 3C and Supplementary Figure S3F, and Student's *t*-test for the other figures. This is because the distributions of the stiffness of the pole and midzone regions were not Gaussian distributions (checked by the normality test).

Biochemical perturbations

The coiled-coil domain 1 (CC1) of dynactin sidearm subunit (p150), referred to as p150-CC1 (a dynein inhibitor), was prepared as described previously [16]. p150-CC1 was added to the extracts immediately after adding fresh metaphase extracts, because the addition of p150-CC1 at this timing is the most effective to suppress pole-focusing function of dynein [17]. Monastrol (an Eg5 inhibitor; M8515, Sigma-Aldrich) was added to the extracts 1 h after adding fresh metaphase extracts. The extracts were incubated at 16°C for 30 min after the addition of monastrol so that the effect of monastrol was saturated. We added these inhibitors in this sequence to examine the effects of dual inhibition of dynein and Eg5.

Results and Discussion

Definition of the pole region and quantitative evaluation of the spindle shape symmetry

We first examined whether or not a pair of pole structures in a spindle is symmetrically organized in shape. Although various MAPs localize near the spindle pole, the boundary between the pole and midzone structures is difficult to precisely determine according to the difference of their compositions (the boundary has not been quantitatively defined). This is because the distribution of pole-localized MAPs, which characterize the mechanical and biochemical properties of the poles, gradually changes from the pole to the equatorial plane [1]. Hence, to investigate whether the boundary could be defined by the shape, we measured the width of spindles at 5–50% of spindle length away from the poles (the position at 50% of spindle length is the equatorial plane of the spindle). We found that the slope of the distance from the pole versus width plots changed when the distance from the pole is at 20% (Fig. 1A). The previous work showed that the velocity of microtubule flux (continuous translocation of the spindle microtubules in the direction from the equatorial plane of the spindle to the pole), is significantly decreased in this region [18]. Accordingly, we defined the region within 20% of the spindle length from the pole as the "pole region". To characterize the shape of this pole region, we calculated the aspect ratio and γ value of the pole region, which depict the ratio of the width to the length of the pole region, and the geometrical shape of the pole region in two dimensions (2D), respectively (γ value of the pole region is calculated as $S/(W_p \times L_p) \times 2$, where S, W_p and L_p are the area,

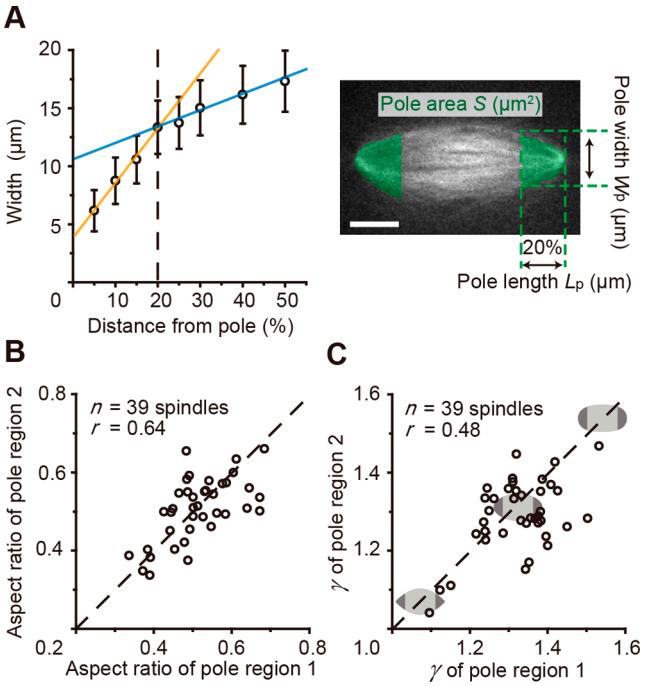

Figure 1 A pair of poles of a spindle is symmetric in shape. (A) The spindle width at 5–50% of spindle length away from the pole (left), and definitions of pole width W_p, pole length L_p and pole area S of the pole region (right). In the left panel, the distance from the pole end is normalized with L (pole-to-pole distance), and each plot includes 28 spindles (error bars, ± S.D.). The orange and blue lines indicate the linear fit (slope: 0.47 and 0.14) for the plots of 5–20% and 20–50% of spindle length away from the pole, respectively. In the right panel, scale bar: 10 μm. (B, C) Comparison of the aspect ratio (B) and γ (C) between pairs of pole regions in single spindles. The aspect ratio and γ of pole regions were calculated as W_p/L_p and $S/(W_p \times L_p) \times 2$, respectively. The numbers 1 and 2 for the pole region labeled on the abscissa and ordinate represent the left and right pole regions in single spindles, respectively. The mean ± S.D. of the aspect ratio and γ value of pole regions were 0.51 ± 0.08 and 1.31 ± 0.09, respectively (n = 78 poles of 39 spindles). The r indicates the correlation coefficient. Schematic illustrations in (C) represent the spindle shape having the corresponding γ values. If the value of γ is 1.0 or 1.57, the pole shape is analogous to a triangle or a half circle, respectively. If the value of γ is between 1.0 and 1.57, the pole shape is analogous to a half ellipse.

width and length of the pole region, respectively. (See also Fig. 1 legend for the definition of these parameters in greater detail, and Supplementary Fig. S1 for microscopic images of the typical spindles with various aspect ratios and the γ values of the pole region). These quantitative analyses revealed that the aspect ratio and the γ value of the pole region were 0.51 ± 0.08 and 1.31 ± 0.09, respectively (mean ± S.D., Fig. 1B, C), i.e., the pole 2D shape was analogous to an ellipse. We defined a normally-shaped spindle as the spindle of which the aspect ratio and the γ value were within the mean ± 3.0 S.D.; that is, the aspect ratio is 0.27–0.75 and the γ value is 1.04–1.58. No significant difference was detected between the pair of pole regions of an individual spindle ($p > 0.5$ for the aspect ratio and $p > 0.05$ for the γ value by Student's *t*-test). These results indicate that elliptically-

shaped poles were formed symmetrically in a spindle.

Mechanical properties of the pole regions

We next examined the mechanical properties such as the elastic stiffness of the pole region and investigated whether or not a pair of pole regions possesses equal stiffness in a spindle. Because the spindle pole is mainly composed of microtubules and crosslinking proteins, the elastic stiffness of pole regions should be determined by the rigidity of microtubules, and the spring constant of crosslinking proteins (therefore, the stiffness of pole regions should be enhanced by increasing microtubule density). To measure the elastic stiffness of pole regions, a stiff glass microneedle and force-calibrated flexible glass microneedle were inserted into one side of the pole region, and this pole region was widened by moving the stiff needle at 1 μm/sec (Fig. 2A–C and Supplementary Movie). Immediately after widening of the pole region and measuring the elasticity in one side, these two needles were removed from this pole region (the first pole region), and inserted into the opposite side pole region (the second pole region) to widen in a similar fashion. The measurement of the stiffness of the second pole region was performed within 1 min after the measurement on the first pole region. Notably, the pole region widened in this process started to become narrow just after the removal of the needles, and then it recovered to its original shape within a few seconds (see the left pole in the Supplementary Movie), suggesting that our deformation procedure did not disrupt the pole structure. The force applied to the pole region during the widening could be estimated from the deflection of the force-calibrated flexible needle. We defined the stiffness as the force required to increase the unit distance between these two needles. In all experiments, the force was linearly elevated until the distance between the two needles d reached 2 μm (Fig. 2D), indicating that the pole structure was predominantly elastic for the time period during this deformation (<10 sec) and at this displacement rate (i.e., the displacement rate of the stiff needle, 1 μm/sec), which was consistent with our previous work [8]. Accordingly, we judged that this displacement rate is suitable to measure the elastic stiffness, and we calculated the stiffness from the slope of d versus force plots in which d ranged from 0 to 2 μm. Probably due to such a small deformation, the stiffness of the pole region was not dependent on the spindle size (Fig. 2E, F) or the pole shape (Fig. 2G, H). The stiffness of the pole region was estimated to be 0.84 ± 0.40 nN/μm (mean ± S.D., $n = 39$ poles of 39 spindles), the magnitude of which is comparable with that of the spindle stiffness reported in our previous works [7,8,10]. We found that the stiffness of a pair of pole regions in a spindle is nearly equal (Fig. 2I). This result suggests that a pair of pole regions in a spindle is symmetrical regarding the mechanical property.

Roles of motor proteins in the mechanical properties of the pole regions

We next investigated the role of dynein on the stiffness of the pole region and the shape symmetry. Dynein forms a complex with dynactin to crosslink overlapping microtubules and transport MAPs towards the spindle pole [1,19]. Therefore, the disorganized pole structure under the suppression of dynein functions [17] (Supplementary Fig. S2A middle) is thought to result from the loss of the crosslinking force on microtubules. Although we tried to measure the stiffness of the pole region of the spindles under complete inhibition of dynein functions, the pole structure (Supplementary Fig. S2A middle) was too weak to detect the deflection of the flexible needle during the widening. Therefore, we decided to measure the stiffness of the pole region under partial inhibition of dynein functions. We found that, while the pole structures of over 90% of spindles were collapsed with 400 nM p150-CC1 ($\gamma \simeq 2.0$), about 75% of spindles maintained their normal bipolar shape with 100 nM (Supplementary Fig. S2B left). Thus, we decided to measure the stiffness of pole regions of the normally shaped spindles in the presence of 100 nM p150-CC1 (i.e., we measured the stiffness of pole regions in the spindles having the aspect ratio and the γ value of the pole region which were equal to those of non-treated spindles). We found that, even though the pole shape of the spindles was indistinguishable from a non-treated spindle (Fig. 3A, B left) and the shape symmetry of these spindles was retained (correlation coefficient $r = 0.48$ for aspect ratio and 0.53 for γ, $n = 35$ spindles; Fig. 3A, B left), the mean stiffness of the pole region was reduced by 73% (0.84 to 0.23 nN/μm, Fig. 3C). The symmetry of the reduced stiffness of the pole region was maintained (correlation coefficient $r = 0.60$, Fig. 3D). The reduction of the stiffness of pole regions should reflect the loss of the crosslinking force between microtubules. Therefore, these results suggest that the spindle poles can adapt to the change of forces applied to their structure, so that their shape and symmetry are maintained.

Complete inhibition of dynein functions dramatically changed the pole shape, but not the spindle width (Supplementary Fig. S2A middle). Therefore, we assumed that the inhibition of the dynein function may be less effective on the stiffness of the midzone. To test this assumption, we measured the stiffness of the midzone region in the presence of 100 nM p150-CC1. The midzone region was defined as the region within ± 10% of the spindle length from the spindle equatorial plane. The stiffness of the midzone region was measured by widening this region using the stiff and flexible needles (Supplementary Fig. S3A). Similar to the stiffness of the pole region, the stiffness of the midzone region was not dependent on the spindle size (Supplementary Fig. S3B, C) or the pole shape (Supplementary Fig. S3D, E). We found that, while suppressing dynein function reduced the mean stiffness of pole regions by 73% (0.84 to 0.23 nN/μm, Fig. 3C), it decreased the mean stiffness of the midzone region by 50% (0.49 to 0.24 nN/μm, Supplementary Fig. S3F, G).

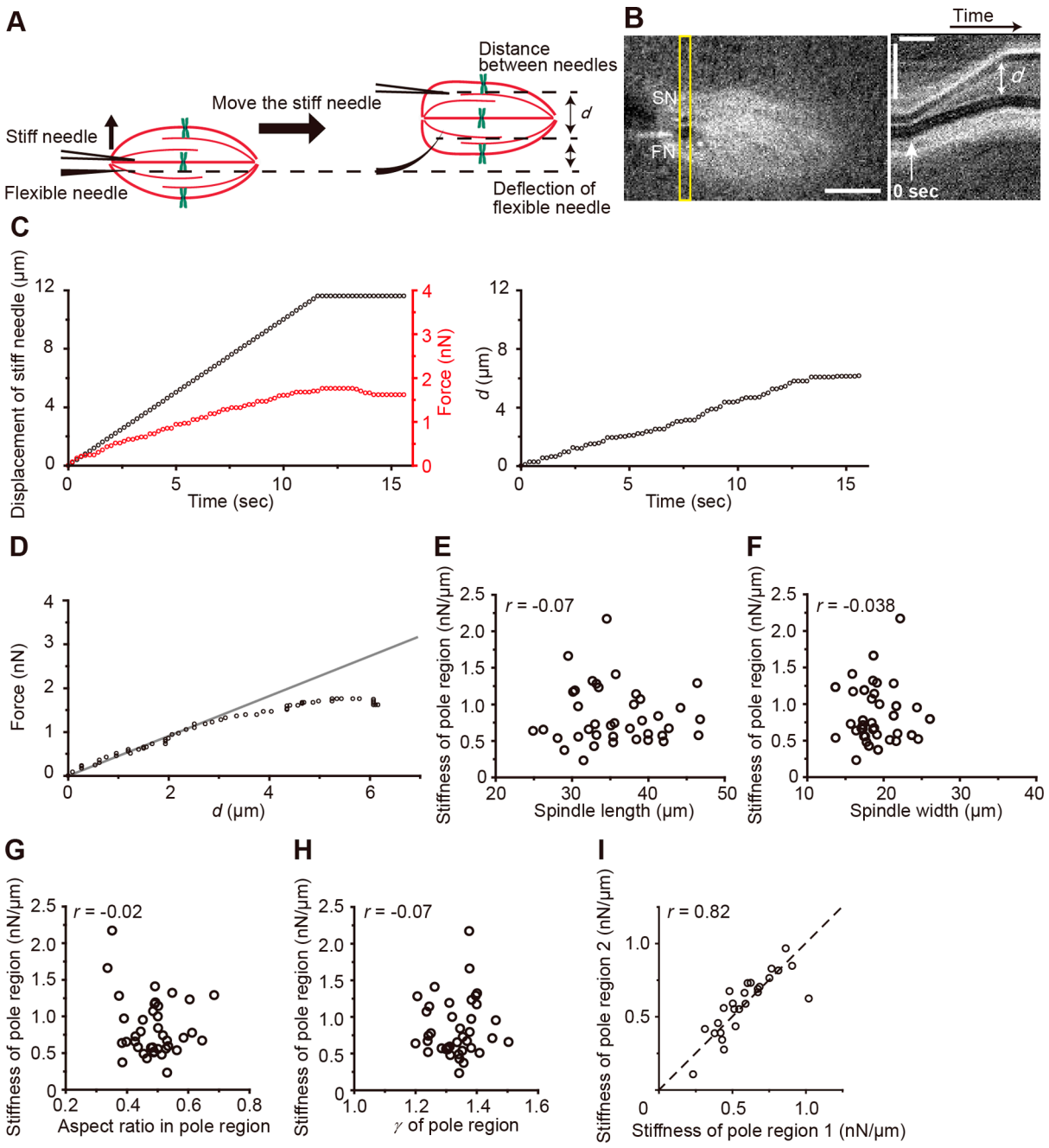

Figure 2 Stiffness of a pair of pole regions is symmetrical in a spindle. (A) Schematic illustration and (B) microscopic images of the spindle and glass microneedles during measurement of the stiffness of the pole region. In (B), SN and FN in the left image indicate stiff and flexible needles, respectively. The right image is the kymograph of the region within the yellow box in the left image. In the left image, scale bar: 10 μm. In the kymograph, scale bars: 10 μm (vertical) and 4 sec (horizontal). (C) Time courses of the displacement of the stiff needle and the distance between two needles d, obtained from the manipulation experiment shown in (B). In the left panel, red plots indicate the force estimated from the deflection of the flexible needle, and black plots denote the displacement of the stiff needle. (D) The relationship between d and force determined from the deflection of the flexible needle shown in (B). The grey line indicates the linear fit for the plots in the region where d was 0–2 μm. The stiffness of the pole region was calculated from the slope of the d versus force plot in the region where d was 0–2 μm, because the force had a linear correlation with d in this region. (E–H) The dependencies of the stiffness of the pole region on spindle length (E), spindle width (width at the equatorial plane of the spindle) (F), the aspect ratio of the pole region (G) and γ (H) of the pole region. The r indicates the correlation coefficient. We examined $n = 39$ poles of 39 spindles (one pole of each spindle). (I) Comparison of the stiffness between pairs of pole regions in single spindles. The numbers 1 and 2 for the pole region labeled on the abscissa and ordinate represent the left and right pole regions in single spindles, respectively.

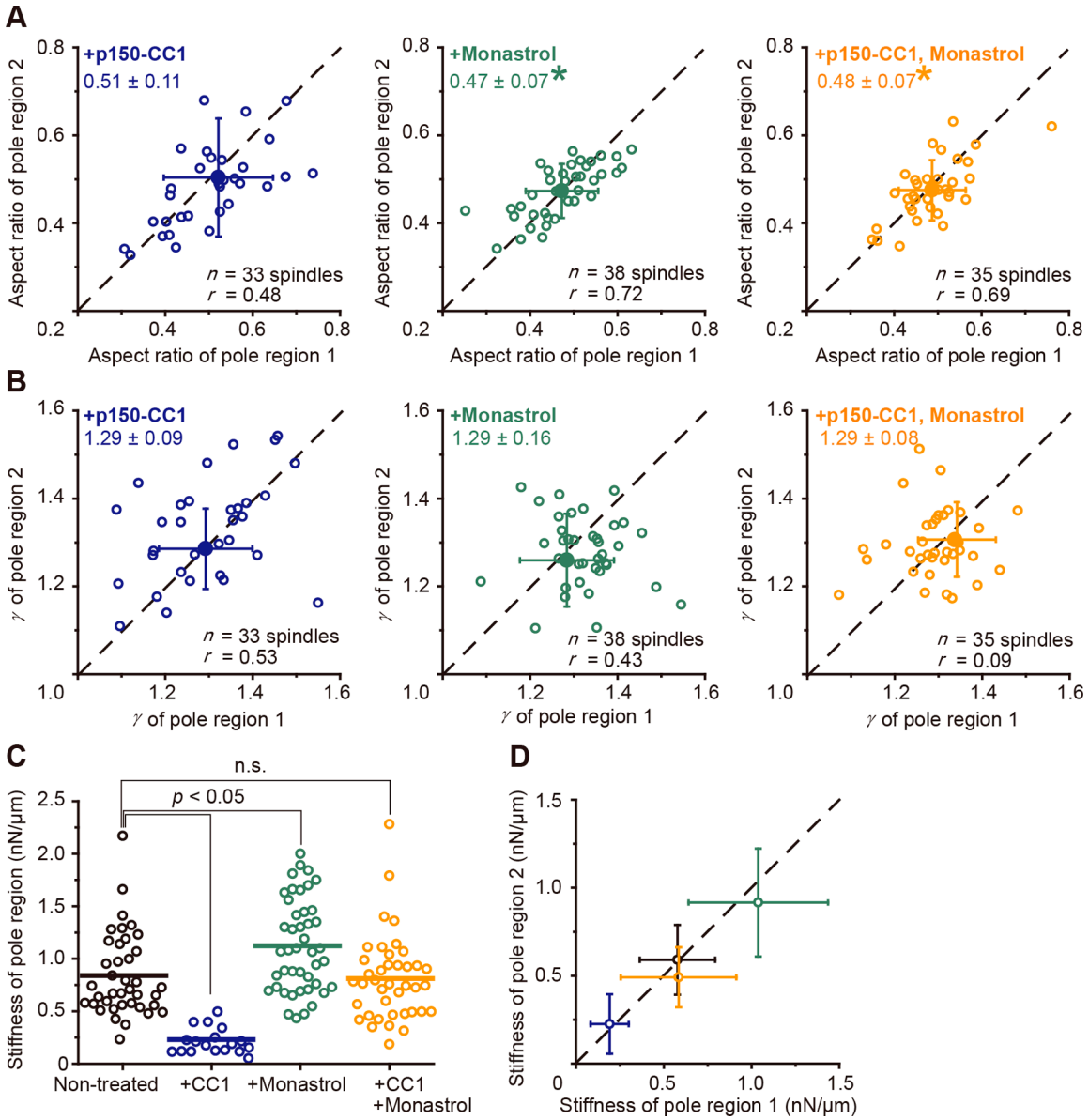

Figure 3 Dynein and Eg5 are involved in the maintenance of the mechanical strength of spindle poles. In all panels, blue, green and orange colors represent p150-CC1- (dynein inhibitor), monastrol- (Eg5 inhibitor) and p150-CC1 and monastrol-treated spindles, respectively. (A, B) Comparison of the aspect ratio (A) and the γ value (B) between pairs of pole regions in single spindles in the presence of p150-CC1 and monastrol. The numbers 1 and 2 for the pole region labeled on the abscissa and ordinate represent the left and right pole regions in single spindles, respectively. Mean ± S.D. is shown in the upper left corners (the mean ± S.D. with the asterisk means that the value is significantly different from that of non-treated spindles, $p < 0.05$ by Student's t-test). Closed circles represent the mean values. (C) The stiffness of the pole region in the presence of inhibitors. Solid lines indicate the mean values. Mean ± S.D.; 0.84 ± 0.40 (non-treated), 0.23 ± 0.14 (p150-CC1), 1.12 ± 0.44 (monastrol) and 0.81 ± 0.41 (both p150-CC1 and monastrol). $n = 39$ (non-treated), 18 (p150-CC1), 44 (monastrol) and 40 (both p150-CC1 and monastrol) spindles. n.s. (not significant): $p > 0.1$ by Mann–Whitney U test. (D) Comparison of the stiffness between pairs of pole regions in single spindles. $n = 26$ (non-treated), 15 (p150-CC1), 15 (monastrol) and 11 (both p150-CC1 and monastrol) spindles. The correlation coefficients are 0.82 (non-treated), 0.60 (p150-CC1), 0.44 (monastrol) and 0.80 (both p150-CC1 and monastrol). The plots represent mean values (error bars, ± S.D.). The r indicates the correlation coefficient.

This result could reflect the difference of the distribution of crosslinking proteins between the pole and midzone regions [1,17,20,21].

Complete inhibition of dynein functions disorganized the pole structures, but the additional inhibition or depletion of Eg5 recovered the pole structures [22]. This fact implicates that Eg5 and dynein antagonistically contribute to the pole formation, i.e., in contrast to dynein, Eg5 might weaken the stiffness of the pole region [23]. To verify this implication quantitatively, we measured the stiffness of the pole region

in the presence of an Eg5 inhibitor (monastrol) which allosterically prohibits Pi release from Eg5, leading to a loss of its sliding force (Supplementary Fig. S2A top) [24,25]. To avoid the effects of the monastrol-induced shape change on our stiffness measurement (generally, the spring constant depends on the shape), we sought to first determine the appropriate concentration of monastrol where spindles maintain their bipolar shape, similar to the p150-CC1-treatment experiments. We found that, while over 90% of spindles were monopolar at 100 μM monastrol, about 75% of spindles maintained their bipolar shape at 25 μM (Supplementary Fig. S2B right). Thus, we decided to measure the stiffness of pole regions in the presence of 25 μM monastrol. The shape symmetry was maintained (correlation coefficient $r = 0.72$ for the aspect ratio and 0.43 for γ, Fig. 3A, B middle). On the other hand, compared with non-treated spindles, the γ value of pole regions did not change ($p > 0.3$, Fig. 3B), but the aspect ratio of pole regions was markedly decreased from 0.51 to 0.47 ($p < 0.05$, Student's *t*-test, Fig. 3A). We considered that this difference did not significantly affect our measurement of the stiffness, because the stiffness of the pole region was independent of the aspect ratio of the pole region (Fig. 2G). As expected, the inhibition of Eg5 with monastrol enhanced the mean stiffness of pole regions by 33% (0.84 to 1.12 nN/μm, Fig. 3C), and the symmetry in the pole stiffness was retained ($r = 0.44$, Fig. 3D). In the presence of 25 μM monastrol, the flux velocity of microtubules was about one-half of that in non-treated spindles [26], thus the stiffness of the pole region might be enhanced by lowering the fluidity of spindle microtubules, as shown in actomyosin networks [27]. In this context, monastrol is more effective in the midzone region, because the velocity of the microtubule flux in the midzone region is higher than that in the pole region [18]. The degree of the monastrol-induced increment of the stiffness of the midzone region (83%; 0.49 to 0.89 nN/μm, Supplementary Fig. S3F, G) was consistently higher than that of the pole region.

Additional inhibition of Eg5 with dynein recovered not only the pole shape, but also the stiffness of the overall spindle structure [8]. This result suggests that, although the mechanism is unclear, the formation of the spindle pole may be closely related to the elasticity of the whole spindle. However, whether or not the stiffness of the pole region itself is also restored under the dual inhibition of dynein and Eg5 remains unknown. To resolve this question, we quantitatively analyzed the pole shape and measured the stiffness of the pole region in the presence of 100 nM p150-CC1 and 25 μM monastrol. The mean aspect ratio of the pole region was slightly changed under the dual inhibition (0.51 to 0.48, Fig. 3A right), but we concluded that the effects of such a shape difference on the stiffness of the pole region can be disregarded based on the same reason as under the suppression of only Eg5 (i.e., the stiffness of the pole region was independent of the aspect ratio of the pole region ranging from 0.27 to 0.75, Fig. 2G). While the correlation coefficient r of the aspect ratio of the pole regions did not significantly change (non-treated: $r = 0.64$; Fig. 1B, treated with both inhibitors: $r = 0.69$; Fig. 3A orange plots), that of γ value of the pole region dramatically decreased (non-treated: $r = 0.48$; Fig. 1C, treated with both inhibitors: $r = 0.09$; Fig. 3B orange plots). This fact means that the shape symmetry of the spindle was disrupted, compared to the non-treated spindles. Inhibition of either dynein or Eg5 did not break the shape symmetry (Fig. 3B), so this result implies that the shape symmetry is maintained in a redundant manner, that is, dynein and Eg5 can compensate for each other to robustly sustain the shape symmetry. We found that the stiffness of dual-inhibited spindle pole regions (0.81 ± 0.40 nN/μm, mean ± S.D., $n = 40$ poles of 40 spindles) was nearly equal to that of non-treated spindle pole regions (0.84 ± 0.40 nN/μm, Fig. 3C). Contrary to the stiffness of the pole region, the stiffness of the midzone region under the dual inhibition (0.78 ± 0.40 nN/μm) was significantly higher than the stiffness of the non-treated spindle midzone region (0.49 ± 0.32 nN/μm, Supplementary Fig. S3F, G). This could be explained from the results that the effects of p150-CC1 and monastrol on the stiffness differ between the midzone and pole regions (Fig. 3C and Supplementary Fig. S3F, G). Taken together, dynein and Eg5 have an antagonistic relationship, that is, dynein and Eg5 function to stiffen and weaken the pole structure, respectively.

Relationship between the stiffness and microtubule density of the pole region

Inhibitor treatment experiments demonstrated that, whereas dynein inhibition weakened the pole structure, Eg5 inhibition stiffened the pole structure. Meanwhile, the stiffness of the overall spindle structure increased with the microtubule density [8]. The previous report raises another possibility that the inhibitor-induced changes of the crosslinking dynamics could modulate the microtubule density in the pole region, leading to the changes in the stiffness of pole regions as detected in the present experiments. To determine whether or not 100 nM p150-CC1 and 25 μM monastrol change the microtubule density in the pole region, we measured the tubulin density in the spindle as we previously reported: we performed a 3D observation of a spindle and measured the volume of the pole or midzone region V, and the amount of tubulin in the pole or midzone region M based on the fluorescence intensity of the fluorescent labeled tubulin incorporated into the microtubules [10,13]. We estimated the mean density (D) of microtubules in the pole and midzone regions, according to $D = M/V$. Note that the density of microtubules we estimated was a relative value and not the actual value. We found that the D value in the pole region changed in a similar manner to the stiffness of the pole region, namely, dynein inhibition decreased the mean value of D by 25% (79 to 59 a.u./μm^3), Eg5 inhibition increased it by 43% (79 to 113 a.u./μm^3), and dual inhibition recovered D to the value of the non-treated spindle poles (79 to 79 a.u./μm^3, Fig. 4A). The D value was nearly equal in the two pole regions of individual spindles, independent of the presence of the inhib-

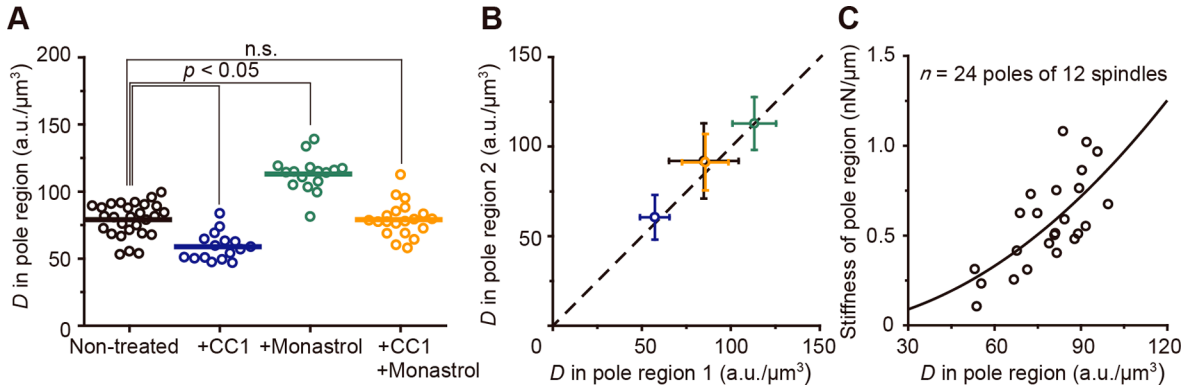

Figure 4 Dynein and Eg5 regulate microtubule density in the pole region. In all panels, black, blue, green and orange colors represent non-treated, p150-CC1, monastrol and both of p150-CC1 and monastrol-treated spindles, respectively. (A) Microtubule density D in the pole region: 28 poles of 14 spindles (non-treated), 16 poles of 8 spindles (p150-CC1), 16 poles of 8 spindles (monastrol) and 20 poles of 10 spindles (both p150-CC1 and monastrol). n.s. (not significant): $p > 0.1$ by Student's t-test. (B) Comparison of microtubule density D between pairs of pole regions in single spindles. The numbers 1 and 2 for the pole region labeled on the abscissa and ordinate represent the left and right pole regions in single spindles, respectively. $n = 19$ spindles (non-treated), 8 spindles (p150-CC1), 8 spindles (monastrol) and 10 spindles (both p150-CC1 and monastrol). Error bars, ± S.D. (C) Relationship between microtubule density D and the stiffness of the pole region. The solid curve indicates the best fit by the stiffness ($= a \times D^b$ where $a = 1.34 \times 10^{-4}$ and $b = 1.91$).

itors (Fig. 4B). If the stiffness of the pole region is dependent only on the microtubule rigidity, the stiffness would increase linearly with microtubule density D [28]. To examine this possibility, we tried to fit the stiffness versus the microtubule density relationship (Fig. 4C) with D^b, and determined the value of b. As a result, the best fit value of b was 1.91, which was consistent with the previous work [12]. This suggests that the stiffness depends not only on the microtubule rigidity but also on the crosslinking proteins [28]. In the case of dynein inhibition, p150-CC1 reduced the number of crosslinking proteins, which directly decreased the stiffness of the pole region. Additionally, the p150-CC1-treatment lowered the D value, which also contributed to the decrement of the stiffness.

Considering our result that the stiffness was dependent on crosslinking proteins (Fig. 3C, D and Supplementary Fig. S3F, G), the difference in the stiffness between pole and midzone regions could be attributed to the difference of the distributions of crosslinking proteins between the two regions. In fact, although the microtubule density D in the midzone region was nearly equal to that in the pole region (Supplementary Fig. S4; the pole region: 79 ± 12 a.u./μm³, the midzone region: 78 ± 16 a.u./μm³, $n = 14$ spindles), the stiffness of the midzone region was significantly lower than that of the pole region (Supplementary Fig. S3G, the pole stiffness: 0.84 ± 0.34 nN/μm, the midzone stiffness: 0.49 ± 0.32 nN/μm, $n = 39$ spindles). Inhibitor-treated spindles showed similar results (Supplementary Fig. S3G and S4). This stiffness difference is not likely derived from the shape difference between the pole and midzone regions, because the stiffness of both regions is independent of the spindle shape (Fig. 2E, F and Supplementary Fig. S3B, C). Rather, this result supports our conclusion that crosslinking proteins significantly contribute to the stiffness.

Maintenance of the spindle symmetry of the mechanical properties and the shape

We have elucidated that the shape, stiffness and microtubule density of a pair of pole regions are symmetrical in an individual spindle. To examine whether or not such symmetry is dynamically balanced, we widened one pole region using two glass microneedles, maintained it in the widened state and investigated how the shape, stiffness and microtubule density in the other pole region change. It is noteworthy that, an additional stiff needle was placed on the unmanipulated pole region during the widening to avoid incline of the spindle from the focal plane. We found that, when one pole region (manipulated pole region) was held in the widened state (Fig. 5A 0 min, 5B left), the other pole region (unmanipulated pole region) was spontaneously widened to form a barrel-like shape (Fig. 5A 11 min, and 5B left). When the barrel-like shaped spindle was formed, the ratio of the γ value of the unmanipulated pole region to that of the manipulated pole region was 1.00 ± 0.13 (mean ± S.D., $n = 15$ spindles), indicating that the spindles were organized in the symmetric structures, and had thereby adapted to the asymmetrical deformation by the external force.

The spindles spontaneously escaped from the inserted needles, as reported previously [29]. Within 10 min after the escape from the needles, the manipulated pole structure was restored (Fig. 5A 21 min, 5B left). Following the restoration of the manipulated pole structure, the unmanipulated pole structure also recovered, leading to the organization of the bipolar shape (Fig. 5A 43 min, 5B left). The shape recovery of these pole structures was similar to the fusion of two spindles shown in previous works [13,30]. The fusion is mediated by dynein [30], so the shape recovery could be driven mainly by this motor protein. It is not only the pole shape, but also the microtubule density in the pole region

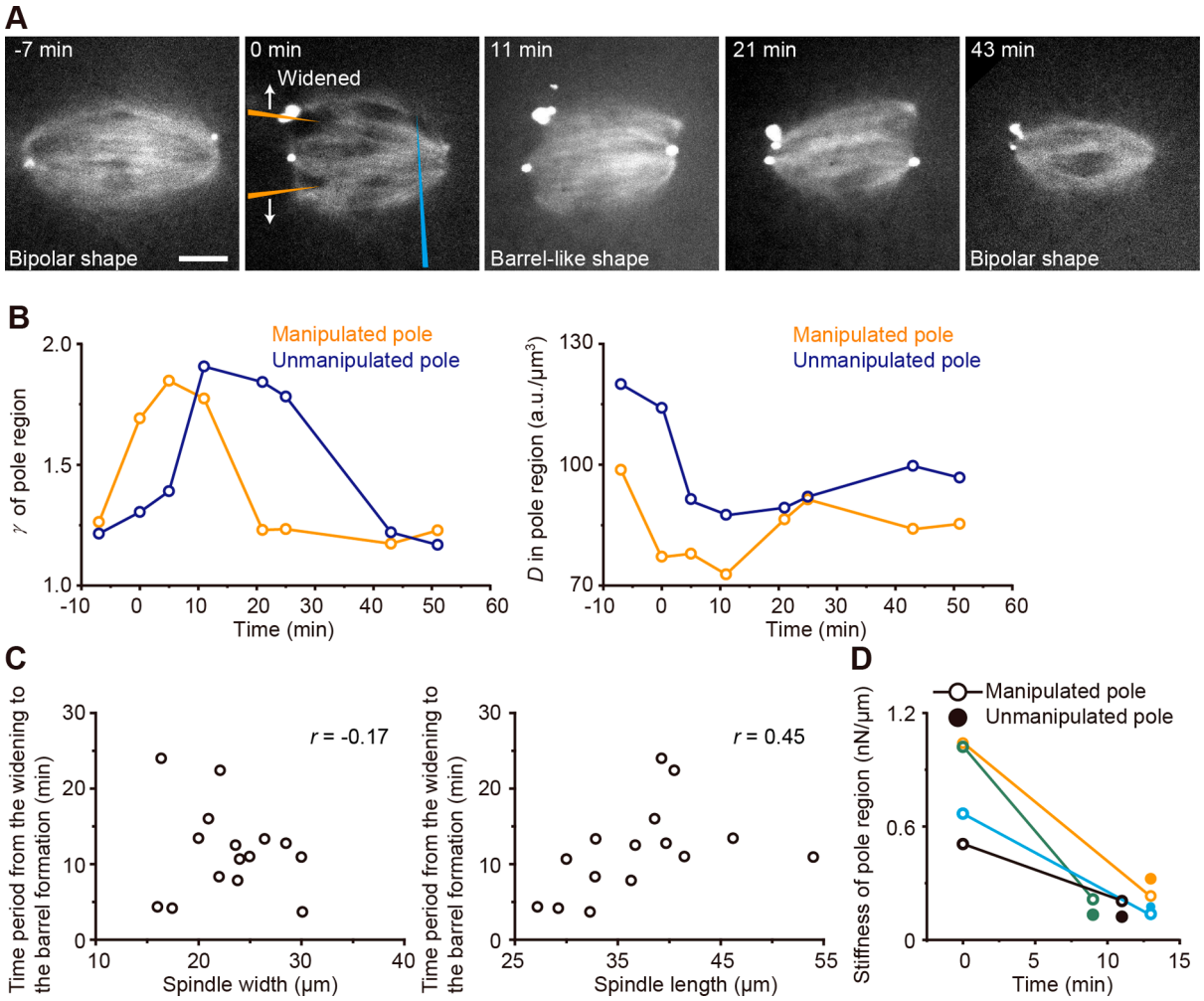

Figure 5 A pair of pole regions in a single spindle is symmetrically balanced in the shape, stiffness and microtubule density. (A) Time-lapse images of the spindle which was held asymmetrically deformed for ~10 min. In the 0 min image, the two orange rods indicate the glass microneedles for the widening, and the blue rod represents the microneedle positioned to avoid incline of the spindle from the focal plane). 0 min: the timing of the start of the widening, Scale bar: 10 μm. (B) Time courses of the γ value (left panel) and the microtubule density D in the pole regions (right panel) in the spindle shown in (A). (C) The relationship between the spindle width (left panel), spindle length (right panel) and the time period from the widening to the timing when the γ value of the unmanipulated pole region became the maximum value during the observation (at this timing, all spindles formed the barrel-like shape as in (A)). $n = 15$ spindles. (D) The stiffness of the pole region before and after the widening of only one pole structure in a single spindle. The same colors indicate the same spindle (e.g., the black open and closed circles indicate the stiffness of the manipulated and unmanipulated pole regions, respectively, in a single spindle). $n = 4$ spindles.

exhibited the similar results. Keeping the widened state with the needles reduced the microtubule density in the manipulated pole region (Fig. 5B right 0 min). Following this reduction, the microtubule density in the unmanipulated pole region also decreased (Fig. 5B right 5 min, see two other examples in Supplementary Fig. S5). This result implies that the unbinding of crosslinking proteins due to the forcible widening of the interaction space of the crosslinking proteins is sequentially transmitted from the manipulated pole to the unmanipulated pole region along the pole-to-pole axis. This consideration is supported from the fact that the time period required for the spindle to recover the symmetrical shape, i.e., a barrel-like structure, was proportional to the spindle length but not to the width (Fig. 5C).

Because the microtubule density was closely related to the stiffness of the pole region (Fig. 4C), we expected that the stiffness of the manipulated pole region would decrease by the widening, and that of the unmanipulated pole region would also decrease. As expected, when the barrel-like shaped spindle was formed by keeping one pole region in the widened state for ~10 min, the stiffness of this manipulated pole region reduced (Fig. 5D open circles), and that of the unmanipulated pole region became nearly equal to that of the manipulated pole region (Fig. 5D closed circles). Note that, we did not measure the stiffness of the unmanipulated pole region before the widening of the manipulated pole region, because the deformation of the pole region reduces its stiffness as seen in the manipulated pole region. Therefore, we

did not have direct evidence showing that the stiffness of the unmanipulated pole region decreased by the widening of the manipulated pole region. However, statistical analysis indicates that, following the decrease in the stiffness of the manipulated pole region, a decrease in the stiffness of the unmanipulated pole region occurs. There is experimental evidence showing a strong correlation of the stiffness between a pair of pole regions (Fig. 2I). Taken together, the present results indicate that there exists a mechanism which dynamically maintains the symmetry of the shape, stiffness and microtubule density of a pair of pole regions in an individual spindle.

Contribution of motor proteins to the maintenance mechanism of the spindle symmetry

The shape symmetry of the spindles was largely disrupted under the suppression of both dynein and Eg5 functions (Fig. 3B orange plots), as compared to non-treated spindles (Fig. 1C) and either dynein- or Eg5-inhibited spindles (Fig. 3B blue, green plots). This result could be derived from the loss of the ability of the spindles to maintain their shape symmetry. To test this consideration, we widened one pole region and held it in the widened state in the presence of both 100 nM p150-CC1 and 25 μM monastrol (the same concentrations as the experiments in Fig. 3B orange plots, where dynein and Eg5 functions are partially inhibited). In this experiment (Supplementary Fig. S6A 0 min, Supplementary Fig. S6B left), the γ value of the other pole region did not change (Supplementary Fig. S6A 22, 32 min, Supplementary Fig. S6B left), contrary to the non-treated spindles (Fig. 5). Namely, even under such a partial suppression condition for both dynein and Eg5, the spindles did not recover their symmetrical shape. The microtubule density of the manipulated pole region decreased within a few minutes after the widening (Supplementary Fig. S6B right), similar to the non-treated spindles (Fig. 5B right and Supplementary Fig. S5A, B right). On the other hand, it took over 20 min for the microtubule density of the unmanipulated pole region to decrease (Supplementary Fig. S6B right). Note that the previous work demonstrated that, after the transient deformation of the spindle by a micromanipulation technique, the microtubule density spontaneously recovered to the original value, which was followed by the recovery of the spindle shape (this process was completed within 4 min after the deformation treatment). This result suggests that the regulation of the microtubule density is important for the maintenance of the spindle shape [10]. Therefore, considering the delay of the start of the decrement of the microtubule density (Supplementary Fig. S6B right), the inhibition of both dynein and Eg5 could impair the ability of the spindle to regulate the microtubule density and to maintain the spindle shape. Although we have not fully understood the detailed mechanism for the maintenance of the symmetry of spindles, it can be concluded that the crosslinking and active-force generation functions of motor proteins are essential. Various kinds of proteins regulating the microtubule density have been identified in addition to dynein and Eg5, for example, Kif2a, MCAK, Augmin, Op18, etc. [17,31–33]. These proteins may also be involved in the mechanism of symmetry maintenance of spindles, which will need to be clarified in future.

Acknowledgments

We gratefully acknowledge Tarun M. Kapoor (Rockefeller University) for providing useful advice on the *Xenopus* egg extract system and for helpful comments, and Jun Takagi (National Institute of Genetics) for fruitful discussions on this work. This research was supported by the Research Fellowship for Young Scientists (DC1) (to K. S.), Grants for Excellent Graduate Schools and Waseda University Grant for Special Research Projects (to K. S.), Grants-in-Aid for Young Scientists (A) (to T. I.) and Scientific Research (S) (to S. I.) from the Ministry of Education, Culture, Sports, Science and Technology of Japan.

Conflict of Interest

The authors declare that they have no conflict of interest.

Author Contributions

K. S. conducted the experiments and data analysis. T. I. prepared p150-CC1. All authors designed the experiments, discussed the results, wrote the manuscript and approved the final version for submission.

References

[1] Walczak, C. E., Vernos, I., Mitchison, T. J., Karsenti, E. & Heald, R. A model for the proposed roles of different microtubule-based motor proteins in establishing spindle bipolarity. *Curr. Biol.* **8**, 903–913 (1998).
[2] Goshima, G., Nédélec, F. & Vale, R. D. Mechanisms for focusing mitotic spindle poles by minus end-directed motor proteins. *J. Cell Biol.* **171**, 229–240 (2005).
[3] Scholey, J. M., Brust-Mascher, I. & Mogilner, A. Cell division. *Nature* **422**, 746–752 (2003).
[4] Gordon, M. B., Howard, L. & Compton, D. A. Chromosome movement in mitosis requires microtubule anchorage at spindle poles. *J. Cell Biol.* **152**, 425–434 (2001).
[5] Oshimori, N., Ohsugi, M. & Yamamoto, T. The Plk1 target Kizuna stabilizes mitotic centrosomes to ensure spindle bipolarity. *Nat. Cell Biol.* **8**, 1095–1101 (2006).
[6] Oshimori, N., Li, X., Ohsugi, M. & Yamamoto, T. Cep72 regulates the localization of key centrosomal proteins and proper bipolar spindle formation. *EMBO J.* **28**, 2066–2076 (2009).
[7] Itabashi, T., Takagi, J., Shimamoto, Y., Onoe, H., Kuwana, K., Shimoyama, I., *et al.* Probing the mechanical architecture of the vertebrate meiotic spindle. *Nat. Methods* **6**, 167–172 (2009).
[8] Shimamoto, Y., Maeda, Y. T., Ishiwata, S., Libchaber, A. J. & Kapoor, T. M. Insights into the micromechanical properties of the metaphase spindle. *Cell* **145**, 1062–1074 (2011).
[9] Itabashi, T., Takagi, J., Suzuki, K. & Ishiwata, S. Responses of

chromosome segregation machinery to mechanical perturbations. *BIOPHYSICS* **9**, 73–78 (2013).
[10] Takagi, J., Itabashi, T., Suzuki, K., Kapoor, T. M., Shimamoto, Y. & Ishiwata, S. Micromechanics of the vertebrate meiotic spindle examined by stretching along the pole-to-pole axis. *Biophys. J.* **106**, 735–740 (2014).
[11] Desai, A., Murray, A., Mitchison, T. J. & Walczak, C. E. The use of Xenopus egg extracts to study mitotic spindle assembly and function in vitro. *Methods Cell Biol.* **61**, 385–412 (1999).
[12] Shimamoto, Y. & Kapoor, T. M. Microneedle-based analysis of the micromechanics of the metaphase spindle assembled in Xenopus laevis egg extracts. *Nat. Protoc.* **7**, 959–969 (2012).
[13] Takagi, J., Itabashi, T., Suzuki, K., Kapoor, T. M., Shimamoto, Y. & Ishiwata, S. Using micromanipulation to analyze control of vertebrate meiotic spindle size. *Cell Rep.* **5**, 44–50 (2013).
[14] Tirnauer, J. S., Salmon, E. D. & Mitchison, T. J. Microtubule plus-end dynamics in Xenopus egg extract spindles. *Mol. Biol. Cell* **15**, 1776–1784 (2004).
[15] Hyman, A., Drechsel, D., Kellogg, D., Salser, S., Sawin, K., Steffen, P., *et al.* Preparation of modified tubulins. *Meth. Enzymol.* **196**, 478–485 (1991).
[16] King, S. J., Brown, C. L., Maier, K. C., Quintyne, N. J. & Schroer, T. A. Analysis of the dynein-dynactin interaction in vitro and in vivo. *Mol. Biol. Cell* **14**, 5089–5097 (2003).
[17] Gaetz, J. & Kapoor, T. M. Dynein/dynactin regulate metaphase spindle length by targeting depolymerizing activities to spindle poles. *J. Cell Biol.* **166**, 465–471 (2004).
[18] Yang, G., Cameron, L. A., Maddox, P. S., Salmon, E. D. & Danuser, G. Regional variation of microtubule flux reveals microtubule organization in the metaphase meiotic spindle. *J. Cell Biol.* **182**, 631–639 (2008).
[19] Heald, R., Tournebize, R., Blank, T., Sandaltzopoulos, R., Becker, P., Hyman, A., *et al.* Self-organization of microtubules into bipolar spindles around artificial chromosomes in Xenopus egg extracts. *Nature* **382**, 420–425 (1996).
[20] Merdes, A., Ramyar, K., Vechio, J. D. & Cleveland, D. W. A complex of NuMA and cytoplasmic dynein is essential for mitotic spindle assembly. *Cell* **87**, 447–458 (1996).
[21] Wittmann, T., Wilm, M., Karsenti, E. & Vernos, I. TPX2, A novel xenopus MAP involved in spindle pole organization. *J. Cell Biol.* **149**, 1405–1418 (2000).
[22] Mitchison, T. J., Maddox, P., Gaetz, J., Groen, A., Shirasu, M., Desai, A., *et al.* Roles of polymerization dynamics, opposed motors, and a tensile element in governing the length of Xenopus extract meiotic spindles. *Mol. Biol. Cell* **16**, 3064–3076 (2005).
[23] Charlebois, B. D., Kollu, S., Schek, H. T., Compton, D. A. & Hunt, A. J. Spindle pole mechanics studied in mitotic asters: dynamic distribution of spindle forces through compliant linkages. *Biophys. J.* **100**, 1756–1764 (2011).
[24] Kapoor, T. M., Mayer, T. U., Coughlin, M. L. & Mitchison, T. J. Probing spindle assembly mechanisms with monastrol, a small molecule inhibitor of the mitotic kinesin, Eg5. *J. Cell Biol.* **150**, 975–988 (2000).
[25] Kwok, B. H., Kapitein, L. C., Kim, J. H., Peterman, E. J., Schmidt, C. F. & Kapoor, T. M. Allosteric inhibition of kinesin-5 modulates its processive directional motility. *Nat. Chem. Biol.* **2**, 480–485 (2006).
[26] Miyamoto, D. T., Perlman, Z. E., Burbank, K. S., Groen, A. C. & Mitchison, T. J. The kinesin Eg5 drives poleward microtubule flux in Xenopus laevis egg extract spindles. *J. Cell Biol.* **167**, 813–818 (2004).
[27] Humphrey, D., Duggan, C., Saha, D., Smith, D. & Käs, J. Active fluidization of polymer networks through molecular motors. *Nature* **416**, 413–416 (2002).
[28] Claessens, M. M., Bathe, M., Frey, E. & Bausch, A. R. Actin-binding proteins sensitively mediate F-actin bundle stiffness. *Nat. Mater.* **5**, 748–753 (2006).
[29] Gatlin, J. C., Matov, A., Danuser, G., Mitchison, T. J. & Salmon, E. D. Directly probing the mechanical properties of the spindle and its matrix. *J. Cell Biol.* **188**, 481–489 (2010).
[30] Gatlin, J. C., Matov, A., Groen, A. C., Needleman, D. J., Maresca, T. J., Danuser, G., *et al.* Spindle fusion requires dynein-mediated sliding of oppositely oriented microtubules. *Curr. Biol.* **19**, 287–296 (2009).
[31] Desai, A., Verma, S., Mitchison, T. J. & Walczak, C. E. Kin I kinesins are microtubule-destabilizing enzymes. *Cell* **96**, 69–78 (1999).
[32] Goshima, G., Mayer, M., Zhang, N., Stuurman, N. & Vale, R. D. Augmin: a protein complex required for centrosome-independent microtubule generation within the spindle. *J. Cell Biol.* **181**, 421–429 (2008).
[33] Belmont, L. D. & Mitchison, T. J. Identification of a protein that interacts with tubulin dimers and increases the catastrophe rate of microtubules. *Cell* **84**, 623–631 (1996).